
Unsteady magnetohydrodynamic casson nanofluid flow through a moving cylinder with brownian and thermophoresis effects

Tanmoy Sarker¹, S. M. Arifuzzaman¹, Sk. Reza-E-Rabbi¹, Rubel Ahmed¹, Md. Shakhaoath Khan^{2,*}, Sarder Firoz Ahmed¹

1. Mathematics Discipline, Khulna University, Khulna 9208, Bangladesh

2. School of Engineering, RMIT University, VIC- 3001, Australia

mohammad.shakhaoath.khan@rmit.edu.au

ABSTRACT. The aim of this study is to analysis of finite difference scheme of unsteady MHD flow of Casson nano-fluid attribute of Brownian motion and thermophoresis through a moving cylinder. The governing model for the flow is metamorphosed into non-dimensional impetus, strength and mass-diffusion equations and evolved numerically by employing explicit finite difference fetch with the aid of a computer programming language Compact visual FORTRAN 6.6a. In order to optimize the strait parameters and exactness of the strait, the stability and convergence test have sustained. It is clear that with primary boundary postulates, $U=V=T=C=0$, and small difference time $\Delta t=0.0005$, $\Delta X=0.202$, and $\Delta R= 0.251$, the strait has converged for Prandtl number, $Pr \geq 0.02$ and Lewis number, $Le \geq 0.018$. The acquired results of this study are discussed for several values of natural parameters viz. Prandtl number, Casson fluid parameter, Lewis number, magnetic parameter, Brownian motion and thermophoresis number on the impetus, strength, mass-diffusion, skin friction, Nusselt number by means of several time steps. Moreover, the graphical representations of the solution are shown by conducting tecplot 9.0.

RÉSUMÉ. Le but de cette étude est d'analyser le schéma de différences finies du flux MHD instable de l'attribut nano-fluide de Casson du mouvement brownien et de la thermophorèse dans un cylindre en mouvement. Le modèle directeur du flux est métamorphosé en équations non dimensionnelles d'impulsion, de force et de diffusion de masse et a évolué numériquement en utilisant la recherche par différence finie explicite à l'aide d'un langage de programmation informatique Compact visual FORTRAN 6.6a. Afin d'optimiser les paramètres et la précision du détroit, les tests de stabilité et de convergence ont été maintenus. Il est clair qu'avec les postulats de limite primaire $U=V=T=C=0$, et une petite différence de temps $\Delta t=0.0005$, $\Delta X=0.202$, et $\Delta R= 0.251$, le détroit a convergé pour le nombre de Prandtl, $Pr \geq 0.02$ et le nombre de Lewis, $Le \geq 0,018$. Les résultats acquis de cette étude sont discutés pour plusieurs valeurs de paramètres naturels, à savoir. Nombre de Prandtl, paramètre de fluide de Casson, nombre de Lewis, paramètre magnétique, mouvement Brownien et numéro de thermophorèse sur l'impulsion, force, diffusion de masse,

frottement de la peau, nombre de Nusselt par plusieurs pas de temps. De plus, les représentations graphiques de la solution sont montrées en effectuant le teplot 9.0.

KEYWORDS: casson fluid, nano particles, EFDM, MHD and Moving cylinder.

MOTS-CLÉS: Fluide de Casson, nanoparticules, EFDM, MHD et cylindre en mouvement.

DOI:10.3166/ACSM.42.181-207 © 2018 Lavoisier

1. Introduction

Nanofluids are treated as a two components mixture made of a base fluid and nanoparticles (1-100 nm). The fundamental characteristics of the nanofluid are the raise of the thermal conductivity of the fluid, minimal impeding in flow passing, extensive stability and equity. In order to get better execution of heat generating, the nano-fluid are utilized in several artificial applications such as chemical production, power generator in power plant, productions of micro-electronics, automotives, advance nuclear system, and nano-drug delivery. Sakiadis (1961) was the pioneer who established the concept of 2D boundary layer flow on continuous solid surface. The basic differential and integral momentum equations of boundary layer theory are governed and these equations are solved for moving continuous flat surface and moving continuous cylindrical surface as well as for both laminar and turbulent flow in the boundary layer.

Choi (1995) was the pathfinder who introduced the term “nanofluid”. Buongiorno (2006) discussed about nano-particles details in convective transport in nano-fluids. Casson fluid (Casson, 1959) is remarkable (e.g., jelly, human blood, tomato sauce and honey and Cancer therapy, fibrinogen, blood cells etc.), are prescribed by a shear thinning fluid that is considered to hold an infinite viscosity when there exist a zero shear rate and flow does not occur for a yield stress below and an infinite shear rate when zero viscosity exists. Mathematics and medical science together with have worked on Casson fluid model. Holding the time-independant properties and exists a certain yield value, Casson fluid model has a great attention in polymer technology. Another examples of similar fluids are human blood near about zero shear rate (Cokelet *et al.*, 1963), blood particles with cylindrical shape (Walwander *et al.*, 1975), xanthan gum liquefaction (Garcia and Casas, 1994) and chocolate (Chevally, 1991). Chocolate and blood are treated as plastic flow of solids which is performed and described by Casson model. Across the space separating two regions of rotating cylinder, Casson fluid was accomplished by Eldabe and Salwa (1995). Aid of Casson model, Okay (1979) explored non-Newtonian blood model with capillaries in vulnerable wall. Employing lattice Boltzmann process, faithful and vibrating blood flow of Casson model was detached by Boyd *et al.* (2007).

In current years, several authors are looked about boundary-layer Casson model due to its wide range of applications. Chemically reacting Casson fluid presence in porous surface has been investigated by Emmanuel *et al.* (2015). Casson nano-fluid over a vertical cylinder which is exponentially stretching has been discussed by Malik *et al.* (2014). With the help of Laplace transformation, unsteady boundary layer flow

of Casson fluid effects of heat transfer is explained by Hussanan *et al.* (2014). Casson nanofluid with chemical reaction and heat source/sink past a stretching sheet was discussed by Hayat *et al.* (2015). MHD free convection, effects of radiation on a Casson fluid yield a horizontal circular cylinder with partial slip in non-Darcy porous medium with viscous dissipation have been performed by Makanda *et al.* (2015), Mahabaleshwar & Lorenzini (2017), Kataria and Patal (2016); Kataria and Patel (2016) studied solet, heat generation, thermal diffusion radiation, chemical reaction and MHD Casson fluid flow past an oscillating vertical porous plate. Availability of magnetic field, Casson fluid past a shrinking sheet that is exponentially accelerated has been discussed by Nadeem *et al.* (2012). Kumari *et al.* (2011) observed peristaltic pumping Casson model yields an inclined channel. On the other hand, inclined tube with multiple neoplasm Casson model was developed by Sreenadh *et al.* (2011).

To author's best knowledge, the investigation of Magnetohydrodynamic flow of Casson nanofluid past a moving cylinder presence of Brownian and thermophoresis effects have kept unrecognized. Therefore, in line with this knowledge gap, it was thought desirable to investigate this problem and the specific aims of this paper were to:

- a) To establish a mathematical model to investigate Casson fluid model with the effects of magnetic field and nano-particles yields a moving cylinder.
- b) To introduce an explicit finite difference method to solve the governing model is associated with momentum, energy and concentration equations in numerical manner by developing an algorithm in computer programming language Compact visual FORTRAN 6.6a.
- c) To analyse stability and convergence test for the fluid flow system.
- e) To investigate the velocity, temperature, concentration distribution of Casson fluids together with skin friction, Nusselt number, streamlines and isotherms with different physical parameters.

2. Mathematical model

In this study, unsteady magnetohydrodynamic (MHD) current of Casson nanofluid past a vertical cylinder has been concerned also the nanofluids is considered that two-stuff of composition (base fluid and nanoparticle). This model does not contain any chemical reactions or radiation and thermal equilibrium exists in founding fluids. The x axis is chosen towards the cylinder which is upward direction whereas the radial coordinate r is chosen normal to the surface, where the radius of the cylinder is r_0 . An identical external magnetic area B_0 is applied on the cylindrical surface which is occupied to electrically non-conducting. The physical model and co-ordinate strait of this study is displayed in the posterior *figure 1*.

The elementary temperature and pressure of the cylinder is \bar{T}_∞ and \bar{C}_∞ and the primary velocity of the cylinder is u_0 . The increased temperature and concentration of the cylindrical surface are reck of \bar{T}_w and \bar{C}_w respectively, where $\bar{T}_w > \bar{T}_\infty$ and $\bar{C}_w > \bar{C}_\infty$.

Under this assumptions, the flow model is given by ;

Continuity Equation,

$$\frac{\partial(ru)}{\partial x} + \frac{\partial(rv)}{\partial r} = 0 \tag{1}$$

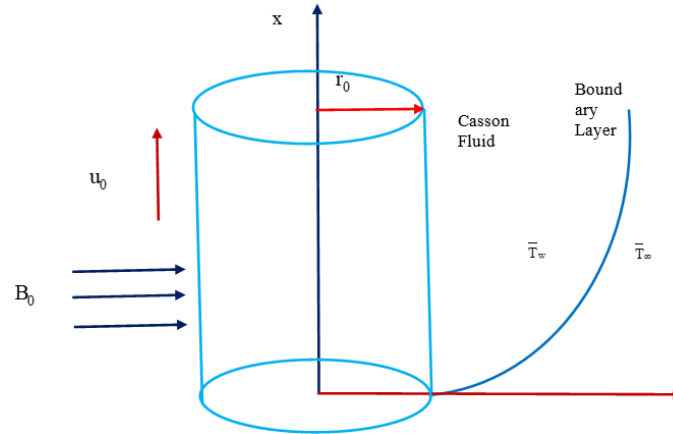


Figure 1. Geometric configuration of flow model

Momentum Equation,

$$\frac{\partial u}{\partial t} + u \frac{\partial u}{\partial x} + v \frac{\partial u}{\partial r} = \nu \left(1 + \frac{1}{\beta} \right) \left(\frac{\partial^2 u}{\partial r^2} + \frac{1}{r} \frac{\partial u}{\partial r} \right) - \frac{\sigma B_0^2}{\rho} u \tag{2}$$

Energy Equation,

$$\frac{\partial \bar{T}}{\partial t} + u \frac{\partial \bar{T}}{\partial x} + v \frac{\partial \bar{T}}{\partial r} = \frac{\kappa}{\rho c_p} \left(\frac{\partial^2 \bar{T}}{\partial r^2} + \frac{1}{r} \frac{\partial \bar{T}}{\partial r} \right) + \tau \left[D_B \frac{\partial \bar{C}}{\partial r} \frac{\partial \bar{T}}{\partial r} + \left(\frac{D_T}{T_\infty} \right) \left(\frac{\partial \bar{T}}{\partial r} \right)^2 \right] \tag{3}$$

Concentration Equation,

$$\frac{\partial \bar{C}}{\partial t} + u \frac{\partial \bar{C}}{\partial x} + v \frac{\partial \bar{C}}{\partial r} = D_B \left(\frac{\partial^2 \bar{C}}{\partial r^2} + \frac{1}{r} \frac{\partial \bar{C}}{\partial r} \right) + \left(\frac{D_T}{T_\infty} \right) \left(\frac{\partial^2 \bar{T}}{\partial r^2} + \frac{1}{r} \frac{\partial \bar{T}}{\partial r} \right) \tag{4}$$

The boundary conditions are,

$$\left. \begin{aligned}
 \bar{t} \leq 0: & \quad u = 0, v = 0, \bar{T} = \bar{T}_\infty, \bar{C} = \bar{C}_\infty && \text{for all } x \geq 0 \text{ and } r \geq 0 \\
 \bar{t} > 0: & \quad u = u_0, v = 0, \bar{T} = \bar{T}_w, \bar{C} = \bar{C}_w && \text{at } r = r_0 \\
 & \quad u = 0, v = 0, \bar{T} = \bar{T}_\infty, \bar{C} = \bar{C}_\infty && \text{at } x = 0 \text{ and } r \geq r_0 \\
 & \quad u \rightarrow 0, \bar{T} \rightarrow \bar{T}_\infty, \bar{C} \rightarrow \bar{C}_\infty && \text{as } r \rightarrow \infty
 \end{aligned} \right\} \quad (5)$$

where u and v indicate the velocity ingredients along the x and r directions, β , the material parameter, ν is the kinematic viscosity, B_0 , the applied magnetic field, ρ , the density of fluid, κ , the thermal conductivity, c_p , the specific heat, $\tau=(\rho c)_p(\rho c)_f$, the ratio of nanoparticle heat capacity to the fluid heat capacity, D_B , Brownian diffusion coefficient, D_T , the thermophoresis diffusion coefficient and Le , the Lewis number. In order to make non-dimensional form from dimensional equations, the subsequent dimensionless contents are introduced,

$$X = \frac{x\nu}{u_0 r_0^2}, \quad R = \frac{r}{r_0}, \quad U = \frac{u}{u_0}, \quad V = \frac{v r_0}{\nu}, \quad t = \frac{\bar{t}\nu}{r_0^2}, \quad T = \frac{\bar{T} - \bar{T}_\infty}{\bar{T}_w - \bar{T}_\infty}, \quad C = \frac{\bar{C} - \bar{C}_\infty}{\bar{C}_w - \bar{C}_\infty} \quad (6)$$

Using the preceding non-dimensional contents, the governing model Eqs. (1)-(4) reduce into the dimensionless form,

Continuity Equation,

$$\frac{\partial(RU)}{\partial X} + \frac{\partial(RV)}{\partial R} = 0 \quad (7)$$

Momentum Equation,

$$\frac{\partial U}{\partial t} + U \frac{\partial U}{\partial X} + V \frac{\partial U}{\partial R} = \left(1 + \frac{1}{\beta}\right) \left(\frac{\partial^2 U}{\partial R^2} + \frac{1}{R} \frac{\partial U}{\partial R} \right) - MU \quad (8)$$

Energy Equation,

$$\frac{\partial T}{\partial t} + U \frac{\partial T}{\partial X} + V \frac{\partial T}{\partial R} = \frac{1}{Pr} \left(\frac{\partial^2 T}{\partial R^2} + \frac{1}{R} \frac{\partial T}{\partial R} \right) + Nb \left(\frac{\partial T}{\partial R} \right) \left(\frac{\partial C}{\partial R} \right) + Nt \left(\frac{\partial T}{\partial R} \right)^2 \quad (9)$$

Concentration Equation,

$$\frac{\partial C}{\partial t} + U \frac{\partial C}{\partial X} + V \frac{\partial C}{\partial R} = \frac{1}{Le} \left\{ \left(\frac{\partial^2 C}{\partial R^2} + \frac{1}{R} \frac{\partial C}{\partial R} \right) + \left(\frac{Nt}{Nb} \right) \left(\frac{\partial^2 T}{\partial R^2} + \frac{1}{R} \frac{\partial T}{\partial R} \right) \right\} \quad (10)$$

And the corresponding boundary postulates in terms of dimensionless variables are,

$$\begin{aligned}
 t \leq 0: U = 0, V = 0, T = 0, C = 0 & \quad \text{everywhere} \\
 t > 0: U = 1, V = 0, T = 1, C = 1 & \quad \text{at } R = 1 \\
 U = 0, V = 0, T = 0, C = 0, & \quad \text{at } X = 0 \text{ and } R \geq 1 \\
 U \rightarrow 0, V \rightarrow 0, T \rightarrow 0, C \rightarrow 0 & \quad \text{at } R \rightarrow \infty
 \end{aligned} \tag{11}$$

where, the obtained physical parameter are given bellow,

Magnetic parameter, $M = \frac{\sigma B_0^2 r_0^2}{\rho \nu}$, Prandtl number, $Pr = \frac{\rho c_p \nu}{\kappa}$, Brownian parameter, $Nb = \frac{\tau D_B (\bar{C}_w - \bar{C}_\infty)}{\nu}$, thermophoresis parameter, $Nt = \frac{\tau D_T (\bar{T}_w - \bar{T}_\infty)}{\bar{T}_\infty \nu}$ and Lewis number, $Le = \frac{\nu}{D_B}$.

The physical non-dimensional quantities namely skin frictions, Nusselt number and Sherwood number are carried out respectively by the subsequent form,

$$Cf = -\frac{1}{2\sqrt{2}} \left(\frac{\partial U}{\partial R} \right)_{R=0} \tag{12}$$

$$Nu = \frac{1}{\sqrt{2}} \left(\frac{\partial T}{\partial R} \right)_{R=0} \tag{13}$$

$$Sh = \frac{1}{\sqrt{2}} \left(\frac{\partial C}{\partial R} \right)_{R=0} \tag{14}$$

Stream function ψ gratifies the continuity equations which are linked directly with velocity ingredients, can be expressed as, $U = \frac{\partial \psi}{\partial Y}$, $V = -\frac{\partial \psi}{\partial X}$.

3. Numerical technique

An explicit finite difference scheme (Khan *et al.*, 2012) is used to detach the governing non-linear partial differential Eqs. (7)-(10) along with boundary postulates Eq. (11). The finite difference equations for Eqs. (7)-(10) are expressed by the Eqs. (15)-(18) respectively. To obtain the finite difference equations, the province of the Casson nanofluid flow is partitioned into the grids or meshes lengthwise to the direction X and R that is apprehend axis and normal to the cylinder (Fig. 2). Here the level of the cylinder is $X_{max} = 20.0$ is considered, i.e X switch from 0 to 20 and $R_{max} = 50.0$ as corresponding to $R \rightarrow \infty$. The subscripts i and j denote the grid points toward the X and R coordinate respectively, where $X = i\Delta X$ and $R = 1 + (j-1)\Delta R$, $M = 100$ and $N = 200$ grid spacing in the X and R directions respectively. The altitude is $\Delta X = 0.202$, $\Delta R = 0.251$ and the small time difference $\Delta t = 0.001$. Let, U', T' and C' represent the worth of U, T and C respectively at ending time step respectively.

By using the explicit finite difference approximation, the following appropriate form are obtained,

$$\frac{U(i, j) - U(i-1, j)}{\Delta X} + \frac{V(i, j) - V(i-1, j)}{\Delta R} + \frac{V(i, j)}{1 + (j-1)\Delta R} = 0 \quad (15)$$

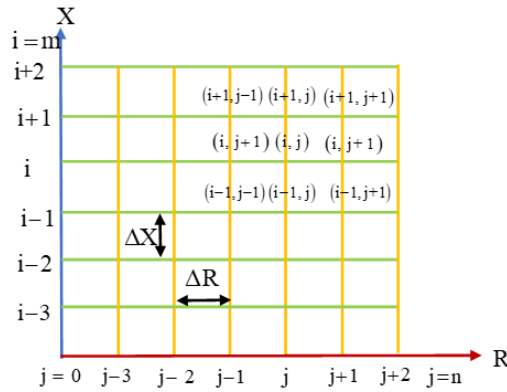


Figure 2. Finite difference space

Momentum equation,

$$\begin{aligned} \frac{U'(i, j) - U(i, j)}{\Delta t} + U(i, j) \frac{U(i, j) - U(i-1, j)}{\Delta X} + V(i, j) \frac{U(i, j+1) - U(i, j)}{\Delta R} &= \left(1 + \frac{1}{\beta}\right) \\ \left\{ \frac{U(i, j+1) - 2U(i, j) + U(i, j-1)}{(\Delta R)^2} + \frac{1}{1 + (j-1)\Delta R} \frac{U(i, j+1) - U(i, j)}{\Delta R} \right\} - MU & \end{aligned} \quad (16)$$

Energy equation,

$$\begin{aligned} \frac{T'(i, j) - T(i, j)}{\Delta t} + U(i, j) \frac{T(i, j) - T(i-1, j)}{\Delta X} + V(i, j) \frac{T(i, j+1) - T(i, j)}{\Delta R} \\ = \frac{1}{Pr} \left\{ \frac{T(i, j+1) - 2T(i, j) + T(i, j-1)}{(\Delta R)^2} + \frac{1}{1 + (j-1)\Delta R} \frac{T(i, j+1) - T(i, j)}{\Delta R} \right\} \\ + Nb \left\{ \frac{T(i, j+1) - T(i, j)}{\Delta R} \right\} \left\{ \frac{C(i, j+1) - C(i, j)}{\Delta R} \right\} + Nt \left\{ \frac{T(i, j+1) - T(i, j)}{\Delta R} \right\}^2 \end{aligned} \quad (17)$$

Concentration equation,

$$\begin{aligned}
 & \frac{C'(i,j)-C(i,j)}{\Delta t} + U(i,j) \frac{C(i,j)-C(i-1,j)}{\Delta X} + V(i,j) \frac{C(i,j+1)-C(i,j)}{\Delta R} \\
 &= \frac{1}{Le} \left\{ \frac{C(i,j+1)-2C(i,j)+C(i,j-1)}{(\Delta R)^2} + \frac{1}{1+(j-1)\Delta R} \frac{C(i,j+1)-C(i,j)}{\Delta R} \right\} \\
 &+ \left(\frac{Nt}{Nb} \right) \left\{ \frac{T(i,j+1)-2T(i,j)+T(i,j-1)}{(\Delta R)^2} + \frac{1}{1+(j-1)\Delta R} \frac{T(i,j+1)-T(i,j)}{\Delta R} \right\} \quad (18)
 \end{aligned}$$

Finally, the primary and boundary postulates becomes the following formations,

When, $t \leq 0$ then, $U_j^0 = 0, T_j^0 = 0, C_j^0 = 0$ everywhere

When, $t > 0$ then, $U_j^0 = 1, T_j^0 = 1, C_j^0 = 1$ for all $R=1$

$$U_j^n = 0, T_j^n = 0, C_j^n = 0 \text{ as } R \rightarrow \infty$$

4. Stability and convergence analysis

To get the solution, an explicit finite difference approximation is applied and the exploration is kept scrappy if not the process of stability test are mentioned. To construct the fixed mesh type, the stability inference are performed as pursue. In general, the clops of the Fourier tract for U, T and C at a time arbitrary namely $t=0$, considered $e^{i\alpha X}$ aloof from a fix value, where $i^2=-1$. At time t, then the term occurs

$$U = F(t)e^{i\alpha X}e^{i\beta R} \quad T = G(t)e^{i\alpha X}e^{i\beta R} \quad C = H(t)e^{i\alpha X}e^{i\beta R} \quad (19)$$

Afterwards, passing a time pas, these terms metamorphose to,

$$U = F'(t)e^{i\alpha X}e^{i\beta R} \quad T = G'(t)e^{i\alpha X}e^{i\beta R} \quad C = H'(t)e^{i\alpha X}e^{i\beta R} \quad (20)$$

After substituting Eqs. (19) and (20) to the Eqs. (15)-(18), we get,

Momentum equation,

$$\begin{aligned}
 & \frac{(F'-F)e^{i\alpha X}e^{i\beta R}}{\Delta t} + U \frac{F(1-e^{-i\alpha\Delta X})e^{i\alpha X}e^{i\beta R}}{\Delta X} + V \frac{F(e^{i\beta R}-1)e^{i\alpha X}e^{i\beta R}}{\Delta R} = \\
 & \left(1 + \frac{1}{\beta} \right) \left\{ \frac{2F(\cos\beta\Delta R-1)e^{i\alpha X}e^{i\beta R}}{(\Delta R)^2} + \frac{1}{R} \frac{F(e^{i\beta\Delta R}-1)e^{i\alpha X}e^{i\beta R}}{\Delta R} \right\} - MFe^{i\alpha X}e^{i\beta R}
 \end{aligned}$$

$$\begin{aligned} \Rightarrow F' &= F \left[1 - U \Delta t \frac{(1 - e^{-i\alpha \Delta X})}{\Delta X} - V \Delta t \frac{(e^{i\beta \Delta R} - 1)}{\Delta R} + \left(1 + \frac{1}{\beta} \right) \left\{ \frac{2(\cos \beta \Delta R - 1)}{(\Delta R)^2} \right. \right. \\ &\quad \left. \left. + \frac{1}{R} \frac{(e^{i\beta \Delta R} - 1)}{\Delta R} \right\} \Delta t - M \Delta t \right] \\ &\Rightarrow F' = A_1 F \end{aligned} \quad (21)$$

where,

$$\begin{aligned} A_1 &= 1 - U \Delta t \frac{(1 - e^{-i\alpha \Delta X})}{\Delta X} - V \Delta t \frac{(e^{i\beta \Delta R} - 1)}{\Delta R} + \left(1 + \frac{1}{\beta} \right) \left\{ \frac{2(\cos \beta \Delta R - 1)}{(\Delta R)^2} \right. \\ &\quad \left. + \frac{1}{R} \frac{(e^{i\beta \Delta R} - 1)}{\Delta R} \right\} \Delta t - M \Delta t \end{aligned}$$

Energy equation,

$$\begin{aligned} &\frac{(G' - G) e^{i\alpha X} e^{i\beta R}}{\Delta t} + U \frac{G(1 - e^{-i\alpha \Delta X}) e^{i\alpha X} e^{i\beta R}}{\Delta X} + V \frac{G(e^{i\beta \Delta R} - 1) e^{i\alpha X} e^{i\beta R}}{\Delta R} \\ &= NbCG \left(\frac{e^{i\beta \Delta R} - 1}{\Delta R} \right)^2 e^{i\alpha X} e^{i\beta R} + \frac{1}{Pr} \left\{ \frac{2G(\cos \beta \Delta R - 1) e^{i\alpha X} e^{i\beta R}}{(\Delta R)^2} \right. \\ &\quad \left. + \frac{1}{R} \frac{G(e^{i\beta \Delta R} - 1) e^{i\alpha X} e^{i\beta R}}{\Delta R} \right\} + NtTG \left(\frac{e^{i\beta \Delta R} - 1}{\Delta R} \right)^2 e^{i\alpha X} e^{i\beta R} \\ &\Rightarrow G' = G \left[1 - U \Delta t \frac{(1 - e^{-i\alpha \Delta X})}{\Delta X} - V \Delta t \frac{(e^{i\beta \Delta R} - 1)}{\Delta R} + \frac{1}{Pr} \left\{ \frac{2(\cos \beta \Delta R - 1)}{(\Delta R)^2} \right. \right. \\ &\quad \left. \left. + \frac{1}{R} \frac{(e^{i\beta \Delta R} - 1)}{\Delta R} \right\} \Delta t + NbC \left(\frac{e^{i\beta \Delta R} - 1}{\Delta R} \right)^2 \Delta t + NtT \left(\frac{e^{i\beta \Delta R} - 1}{\Delta R} \right)^2 \right] \\ &\Rightarrow G' = A_2 G \end{aligned} \quad (22)$$

where,

$$\begin{aligned} A_2 &= 1 - U \Delta t \frac{(1 - e^{-i\alpha \Delta X})}{\Delta X} - V \Delta t \frac{(e^{i\beta \Delta R} - 1)}{\Delta R} + \frac{1}{Pr} \left\{ \frac{2(\cos \beta \Delta R - 1)}{(\Delta R)^2} + \frac{1}{R} \frac{(e^{i\beta \Delta R} - 1)}{\Delta R} \right\} \Delta t \\ &\quad + NbC \left(\frac{e^{i\beta \Delta R} - 1}{\Delta R} \right)^2 \Delta t + NtT \left(\frac{e^{i\beta \Delta R} - 1}{\Delta R} \right)^2 \end{aligned}$$

Concentration equation,

$$\begin{aligned} & \frac{(H' - H)e^{i\alpha X}e^{i\beta R}}{\Delta t} + U \frac{H(1 - e^{-i\alpha\Delta X})e^{i\alpha X}e^{i\beta R}}{\Delta X} + V \frac{H(e^{i\beta\Delta R} - 1)e^{i\alpha X}e^{i\beta R}}{\Delta R} = \\ & \frac{1}{Le} \left\{ \frac{2H(\cos\beta\Delta R - 1)e^{i\alpha X}e^{i\beta R}}{(\Delta R)^2} + \frac{1}{R} \frac{H(e^{i\beta\Delta R} - 1)e^{i\alpha X}e^{i\beta R}}{\Delta R} \right\} + \\ & \left(\frac{Nt}{Nb} \right) \left\{ \frac{2G(\cos\beta\Delta R - 1)e^{i\alpha X}e^{i\beta R}}{(\Delta R)^2} + \frac{1}{R} \frac{G(e^{i\beta\Delta R} - 1)e^{i\alpha X}e^{i\beta R}}{\Delta R} \right\} \\ \Rightarrow H' = & H \left[1 - U\Delta t \frac{(1 - e^{-i\alpha\Delta X})}{\Delta X} - V\Delta t \frac{(e^{i\beta\Delta R} - 1)}{\Delta R} + \frac{1}{Le} \left\{ \frac{2(\cos\beta\Delta R - 1)}{(\Delta R)^2} \right. \right. \\ & \left. \left. + \frac{1}{R} \frac{(e^{i\beta\Delta R} - 1)}{\Delta R} \right\} \right] \Delta t \left(\frac{Nt}{NbLe} \right) \left\{ \frac{2(\cos\beta\Delta R - 1)}{(\Delta R)^2} + \frac{1}{R} \frac{(e^{i\beta\Delta R} - 1)}{\Delta R} \right\} G\Delta t \\ \Rightarrow H' = & A_3 H + A_4 G \tag{23} \end{aligned}$$

where,

$$\begin{aligned} A_3 = & 1 - U\Delta t \frac{(1 - e^{-i\alpha\Delta X})}{\Delta X} - V\Delta t \frac{(e^{i\beta\Delta R} - 1)}{\Delta R} + \frac{1}{Le} \left\{ \frac{2(\cos\beta\Delta R - 1)}{(\Delta R)^2} + \frac{1}{R} \frac{(e^{i\beta\Delta R} - 1)}{\Delta R} \right\} \Delta t \\ A_4 = & \left(\frac{Nt}{Nb} \right) \left\{ \frac{2(\cos\beta\Delta R - 1)}{(\Delta R)^2} + \frac{1}{R} \frac{(e^{i\beta\Delta R} - 1)}{\Delta R} \right\} \Delta t \end{aligned}$$

Eqs. (21)-(23) can be expressed on the matrix form,

$$\begin{bmatrix} F' \\ G' \\ H \end{bmatrix} = \begin{bmatrix} A_1 & 0 & 0 \\ 0 & A_2 & 0 \\ 0 & A_4 & A_2 \end{bmatrix} \begin{bmatrix} F \\ G \\ H \end{bmatrix} \text{ i.e. } \eta' = T'\eta$$

Δt is very small, so $A_4 \rightarrow 0$. The eigenvalues of the matrix T' are $\lambda_1=A_1$, $\lambda_2=A_2$ and $\lambda_3=A_3$. For stability test, each eigenvalues λ_1 , λ_2 and λ_3 must not exceed unity in modulus, then,

$$|A_1| \leq 1, |A_2| \leq 1 \text{ and } |A_3| \leq 1$$

Let,

$$a_1 = \frac{\Delta t}{R\Delta R}, \quad b_1 = \frac{|U|\Delta t}{\Delta X}, \quad c_1 = \frac{|-V\Delta t|}{\Delta R}, \quad d_1 = \Delta t, \quad e_1 = \frac{2\Delta t}{(\Delta R)^2}$$

Then, we get,

$$A_1 = 1 - b_1(1 - e^{-i\alpha\Delta X}) - c_1(e^{i\beta\Delta R} - 1) + \left(1 + \frac{1}{\beta}\right) \left\{e_1(\cos\beta\Delta R - 1) + a_1(e^{i\beta\Delta R} - 1)\right\} - Md_1$$

$$A_2 = 1 - b_1(1 - e^{-i\alpha\Delta X}) - c_1(e^{i\beta\Delta R} - 1) + \frac{1}{Pr} \left\{e_1(\cos\beta\Delta R - 1) + a_1(e^{i\beta\Delta R} - 1)\right\} - CNb \frac{e_1}{2}(e^{i\beta\Delta R} - 1)^2 - TNt \frac{e_1}{2}(e^{i\beta\Delta R} - 1)^2$$

$$A_3 = 1 - b_1(1 - e^{-i\alpha\Delta X}) - c_1(e^{i\beta\Delta R} - 1) + \frac{1}{Le} \left\{e_1(\cos\beta\Delta R - 1) + a_1(e^{i\beta\Delta R} - 1)\right\}$$

The coefficient of a_1 , b_1 and c_1 are non-negative. So the maximum modulus of A_1 , A_2 and A_3 occurs when $\alpha\Delta X = m\pi$ and $\beta\Delta R = n\pi$, where n is integer. The values of $|A_1|$, $|A_2|$ and $|A_3|$ are greater when m and n both are odd integer, in which case,

$$A_1 = 1 - 2 \left[b_1 + c_1 + \left(1 + \frac{1}{\beta}\right)(e_1 + a_1) + \frac{M}{2}d_1 \right]$$

$$A_2 = 1 - 2 \left[b_1 + c_1 + \frac{1}{Pr}(e_1 + a_1) - CNbe_1 - TNte_1 \right]$$

$$A_3 = 1 - 2 \left[b_1 + c_1 + \frac{1}{Le}(e_1 + a_1) \right]$$

To satisfy probable values are $A_1 = -1$, $A_2 = -1$ and $A_3 = -1$, the stability conditions are,

$$U \frac{\Delta t}{\Delta X} + V \frac{\Delta t}{\Delta R} + \frac{1}{Pr} \left\{ \frac{2\Delta t}{(\Delta R)^2} + \frac{\Delta t}{R\Delta R} \right\} - CNb \frac{2\Delta t}{(\Delta R)^2} - TNt \frac{2\Delta t}{(\Delta R)^2} \leq 1$$

$$U \frac{\Delta t}{\Delta X} + V \frac{\Delta t}{\Delta R} + \frac{1}{Le} \left\{ \frac{2\Delta t}{(\Delta R)^2} + \frac{\Delta t}{R\Delta R} \right\} \leq 1$$

Applying primary boundary postulates, $U=V=T=C=0$, and small time pas $\Delta t=0.0005$, $\Delta X=0.202$, $\Delta R=0.251$, then the model will converge for $Pr \geq 0.02$ and $Le \geq 0.018$. Finally, the convergence and stability solutions have been presented with graph in *figures 3 - 18*.

5. Results and discussions

Two-dimensional laminar boundary layer flow of unsteady, MHD Casson fluid over an moving cylinder has been investigated numerically. To express the physical sagacity into this study, the velocity profiles, temperature profiles, skin friction profiles and Nusselt number have been plotted using several values of the parameters namely Casson fluid parameter β , Prandtl number Pr , magnetic parameter M , Brownian parameter Nb , thermophoresis parameter Nt and Lewis number Le of the cylinder. The value of the main parameters considered as $Pr = 0.71$ (for air), $\beta = 0.7$; 1.4; 2.0; 3.0, $M = 0.0$; 1.0, 2.0, 3.0, $Nb = 0.1$; 2.0; 4.0; 6.0; 8.0, $Nt = 0.1$; 2.0; 4.0; 6.0; 8.0 and $Le = 1.0$; 3.0; 5.0. The outcomes of the above parameters on the velocity profiles, temperature profiles, skin frictions profiles and Nusselt number profiles are represent in figures 3 - 18. In this present work, Casson nano-fluid is studied and evolved by explicit finite difference simulation. With the development in Casson fluid parameter β , the viscosity of the fluid particles raise up which slow down the flow. In figure 3, it is seen that the momentum boundary layer decreases with rising values of Casson fluid parameter β . The decreasing rate of velocity profile from $\beta = 0.7$ to 1.4 is 10%, $\beta = 1.4$ to 2.0 is 3.3% and $\beta = 2.0$ to 3.0 is 2% at $R = 2$. The effect of velocity profile has been shown for changing parameters of magnetic field strength M in figure 4. The results are here kept that the velocity profile decreases with increase of magnetic parameter M .

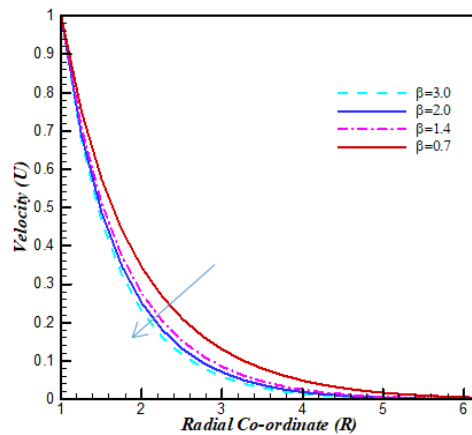


Figure 3. Velocity profiles for various values of β against R when $M = 1.0$, $Pr = 0.71$, $Nb = 0.1$, $Nt = 0.1$ and $Le = 1.0$

Due to the fact that appearance of roundabout magnetic field creates a resistive force on the wall surface. Lorentz force is named after this phenomena, which leads to retard the movement of fluid. The red line shows that Magnetic field strength is absent here. As a results, increment of Magnetic parameter, the momentum thickness falls at the rate of 7.0% from $M=0.0$ to 1.0, 5.0% from $M = 1.0$ to 2.0 and 4.0% from

$M = 2.0$ to 3.0 at $R = 2$. The behavior of the temperature profiles for several values of Brownian parameter Nb are demonstrated in *figure 5*. It is fact that Nb is directly proportional to Brownian diffusion coefficient DB that enhances mass transfer. Therefore growing value of DB increases Nb , which accelerates mass transfer. Also temperature profiles raise with the development of Brownian parameter Nb at the rate of 7% from $Nb = 2.0$ to 4.0 , 4% from $Nb = 4.0$ to 6.0 and 3.5% from $Nb = 6.0$ to 8.0 at $R = 2$. Again the behavior of the temperature profiles for several values of thermophoresis parameter Nt are demonstrated in *figure 6*. As Nt and thermophoresis diffusion coefficient DT are directly proportional, the increasing value of DT increases Nt , which accelerates mass transfer. Then the increasing rate of temperature profile for different values of Nt is 3.3% from $Nt = 0.5$ to 2.0 , 3.0% from $Nt = 2.0$ to 4.0 and 2.5% from $Nt = 4.0$ to 6.0 at $R = 2$. The presence of Prandtl number, Pr , The thermal conductivity of fluid collapse, as a result, thermal boundary layer falls. For this reason temperature profiles decrease due to improvement in Prandtl number, Pr (*figure 7*). The curve to curve decreasing rate is 4.5% from $Pr = 1.0$ to 2.1 , 3.3% from $Pr = 2.1$ to 3.0 and 3.7% from $Pr = 3.0$ to 4.1 at $R = 2$.

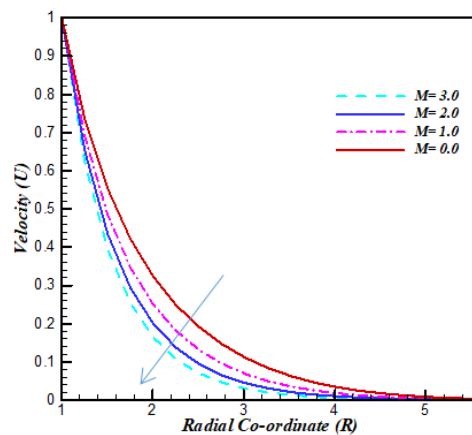


Figure 4. Velocity profiles for various values of M against R when $\beta = 2$, $Pr = 0.71$, $Nb = 0.1$, $Nt = 0.1$ and $Le = 1.0$

Figure 8 evinces the concentration profiles for various worth of thermophoresis parameter Nt . It is executed that with the increase of Nt concentration profiles increase and the increasing rate is 1.5% from $Nt = 0.5$ to 1.0 , 5.0% from $Nt = 1.0$ to 2.0 and 2.5% from $Nt = 2.0$ to 4.0 at $R = 2$. On the other hand, *figure 9* indicates that concentration profiles collapse due to rising value of Lewis number Le . The reason is that Lewis number has opposite properties compared to Brownian diffusion coefficient DB . Then Le increases when DB decreases that is why concentration profiles decrease and the decreasing rate is 14.5% from $Le = 1.0$ to 3.0 , 6.0% from $Le = 3.0$ to 5.0 and 3.0% from $Le = 5.0$ to 7.0 at $R = 2$. The effect of the skin friction has presented in *figure 10-11* for separate values of β and M respectively. For the

amplification of both parameter β and M skin friction falls. With the development of β , viscosity of the fluid rise up, so skin friction decreases. For the strong magnetic parameter, skin friction decreases due to drag force effect. The change of Casson parameter 15.6%, 6.64% and 6.17% decrease for curve to curve at $t=1.0$. Also for the skin friction, the curves fluctuate occur 16.5%, 13.41% and 11.52% decrease at $t=1.0$. Figure 12 represents the Nusselt number for $Pr = 0.71$ is more improvement curve than that of $Pr = 7.0$. The change of Prandtl number, the decreasing rate of Nt is 3.6% from $Pr = 0.71$ to 3.0 and 2.6% from $Pr = 3.0$ to 7.0 at $t=1.0$. Also in figure 13-14 illustrate the Nusselt number for dissimilar values of Nb and Nt respectively.

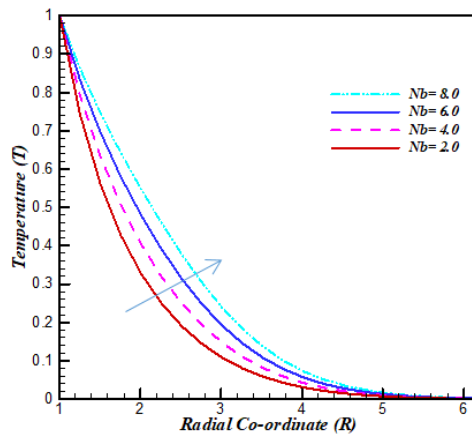


Figure 5. Temperature profiles for various values of Nb against R when $M = 1.0$, $Pr = 0.71$, $\beta = 2.0$, $Nt = 0.1$ and $Le = 1.0$

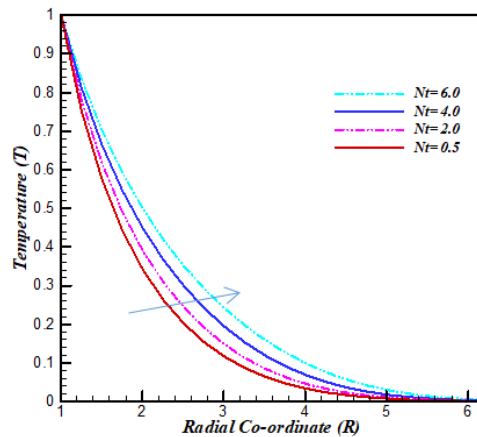


Figure 6. Temperature profiles for various values of Nt against R when $M = 1.0$, $Pr = 0.71$, $\beta = 2.0$, $Nb = 2.0$ and $Le = 1.0$

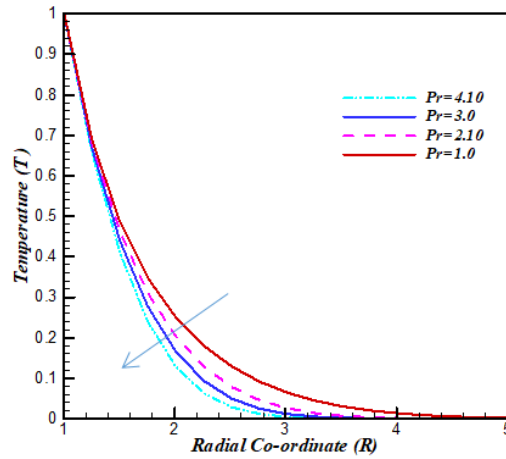


Figure 7. Temperature profiles for various values of Pr against R when $M = 1.0$, $Nt = 0.1$, $\beta = 2.0$, $Nb = 2.0$ and $Le = 1.0$

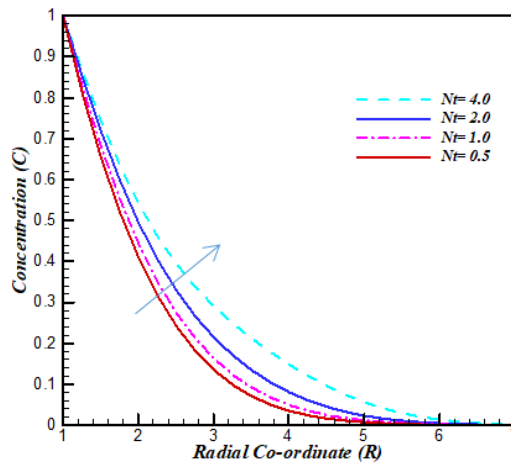


Figure 8. Concentration profiles for various values of Nt against R when $M = 1.0$, $Pr = 0.71$, $\beta = 2.0$, $Nb = 2.0$ and $Le = 1.0$

For both cases, the Nusselt number falls with the development of Brownian parameter and thermophoresis parameter. The change of Brownian parameter, the decreasing rate of Nusselt number is 22% from $Nb = 0.1$ to 0.3 , 21.8% from $Nb = 0.3$ to 0.5 and 21.6% from $Nb = 0.5$ to 0.7 at $t = 1.0$. On the other hand, the curve to curve decreasing rate with the increase of thermophoresis parameter is 18.25% from $Nt = 0.2$ to 0.2 , 17.94% from $Nt = 0.4$ to 0.6 and 17.61% from $Nb = 0.6$ to 0.8 at $t = 1.0$.

The non-dimensional equation has been solved by after different transformations. This is why, X and R axis are dimensionless that indicate the mesh point different from the numerical point of view. Furthermore, streamlines profiles are used to improve visualization of fluid fields. It shows the approach of fluid particle velocity correspondingly. The stream lines may be acquired by marking tangent line to the vexillary. The changing manner of boundary layer can be presented by means of an isotherm, where the constant temperature are assumed. An isotherm at zero degree centigrade is called the freezing level.

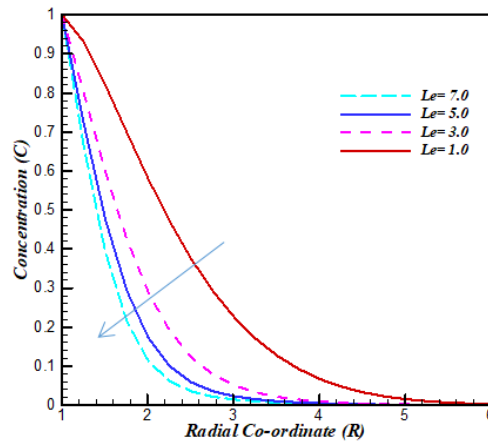


Figure 9. Concentration profiles for various values of Le against R when $M = 1.0$, $Pr = 0.71$, $\beta = 2.0$, $Nb = 2.0$ and $Nt = 0.1$

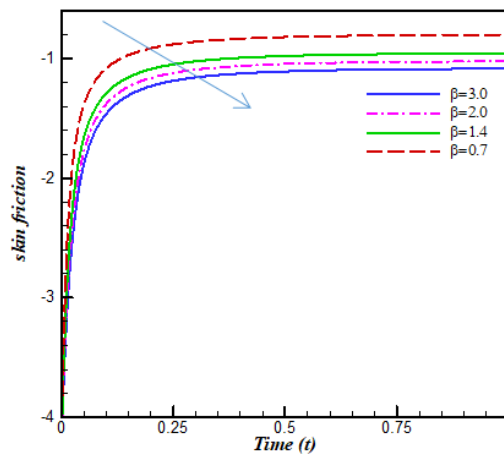


Figure 10. Skin friction profiles for various values of β against t when $M = 1.0$, $Pr = 0.71$, $Nb = 0.1$, $Nt = 0.1$ and $Le = 1.0$

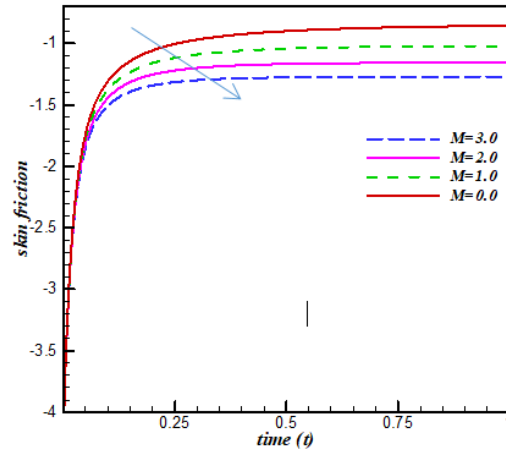


Figure 11. Skin friction profiles for various values of M against t when $Pr = 0.71$, $\beta = 2.0$, $Nb = 0.1$, $Nt = 0.1$ and $Le = 1.0$

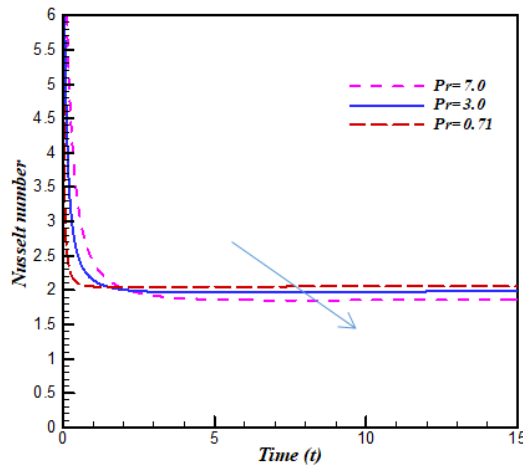


Figure 12. Nusselt number profiles for various values of Pr against t when $M = 1.0$, $\beta = 2.0$, $Nb = 0.1$, $Nt = 0.1$ and $Le = 1.0$

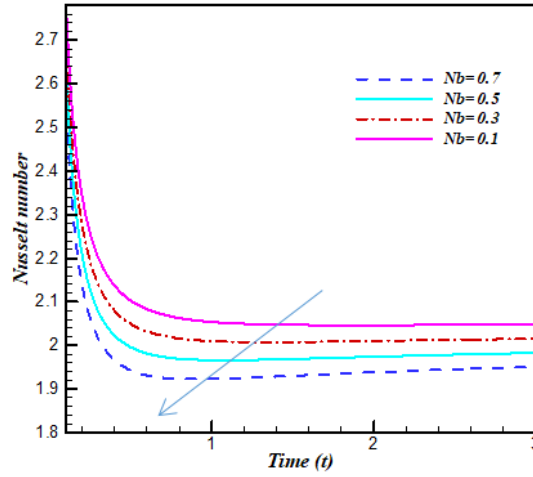


Figure 13. Nusselt number profiles for various values of Nb against t when $Pr = 0.71$, $M = 1.0$, $\beta = 2.0$, $Nt = 0.1$ and $Le = 1.0$

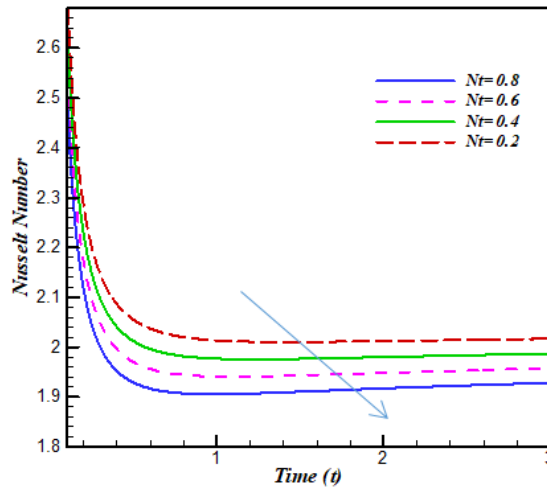


Figure 14. Nusselt number profiles for various values of Nt against t when $Pr = 0.71$, $M = 1.0$, $\beta = 2.0$, $Nb = 0.1$ and $Le = 1.0$

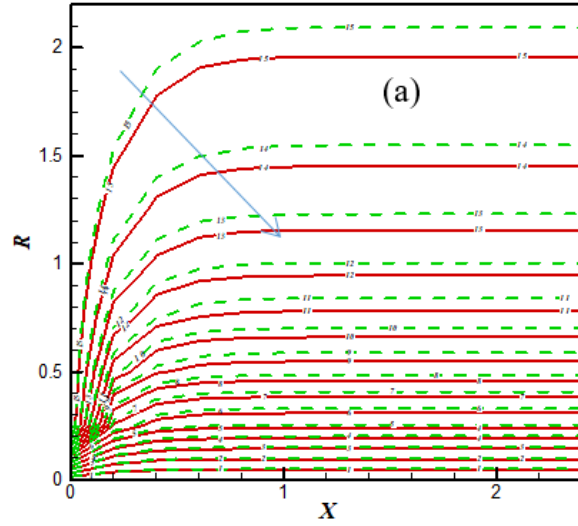


Figure 15. (a) Streamlines for $\beta=3.0$ (red impact line) and $\beta=2.0$ (green dashed line)

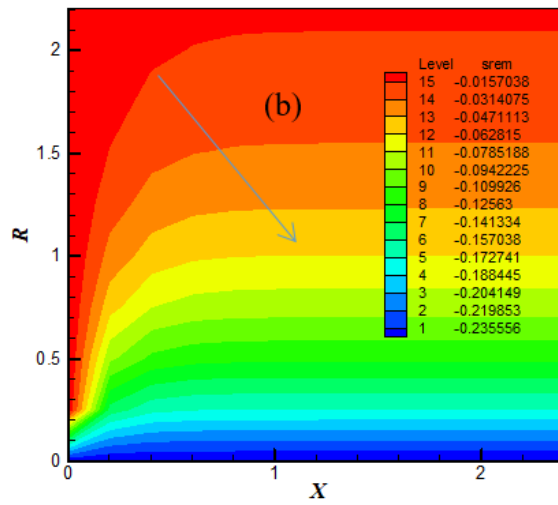


Figure 15. (b) Streamlines flood view

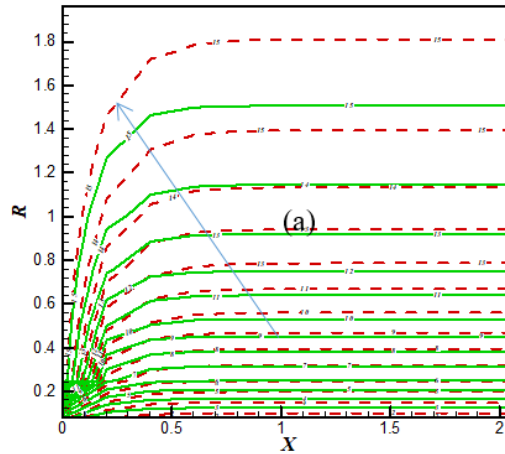


Figure 16. (a) Streamlines for $M = 3.0$ (red dashed line) and $M = 1.0$ (green solid line)

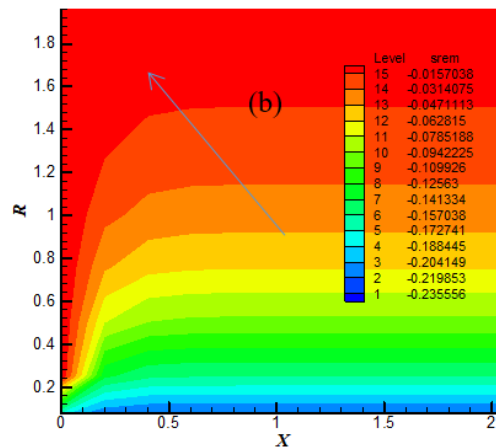


Figure 16. (b) Streamlines flood view

The corepority of streamlines and isotherms have been displayed in *figure 15-16*. Streamlines decreases due to rising values of Casson fluid parameter from $\beta = 2.0$ to $\beta = 3.0$ but develop caused by improvement of magnetic parameter from $M = 1.0$ to $M = 3.0$ in *figure 15(a)-16(a)* respectively.

Again, *figure 15(b)-16(b)* show the contour flood view for difference of Casson fluid parameter and Magnetic parameter respectively. The contours levels are also

provided in the legend of *figure 15(b)-16(b)*. In *figure 17(a)-18(a)*, isotherms lines is seen to be increased with the raise of both Brownian parameter from $Nb = 2.0$ to $Nb = 4.0$ and thermophoresis parameter $Nt = 2.0$ to $Nt = 4.0$. The legend values of *figure 17(b)-18(b)* are given in the contour levels. On the other hand, isotherms lines decreases for various values of Prandtl number from $Pr = 1.2$ and $Pr = 2.1$ in *figure 19(a)-19(b)* shows the contour flood view for difference of Prandtl number. Table 2. shows the numerical values of skin friction and Nusselt number effects of Casson fluid parameter and Magnetic parameter, It is clear that skin friction falls for the both rising values β and M where the is no effect in local Nusselt number.

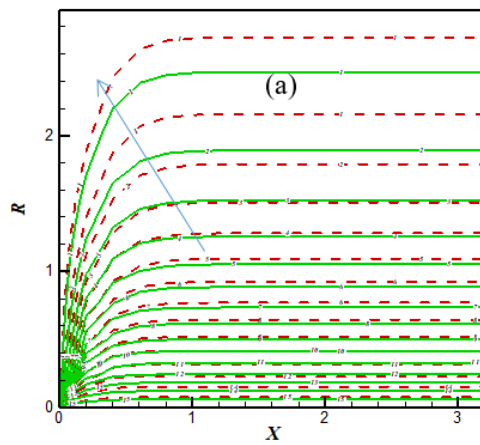


Figure 17. (a) Isotherms for $Nb = 4.0$ (red dashed line) and $Nb = 2.0$ (green solid line)

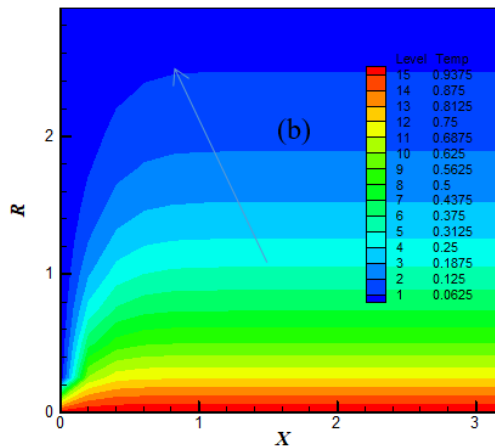


Figure 17. (b) Isotherms flood view

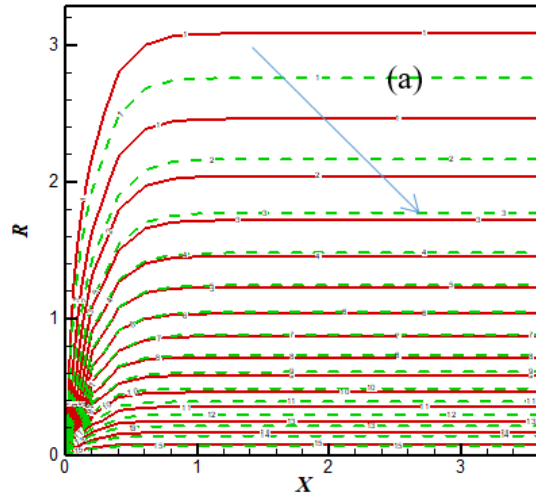


Figure 18. (a) Isotherms for $Nt = 4.0$ (red impact line) and $Nt = 2.0$ (green dashed line)

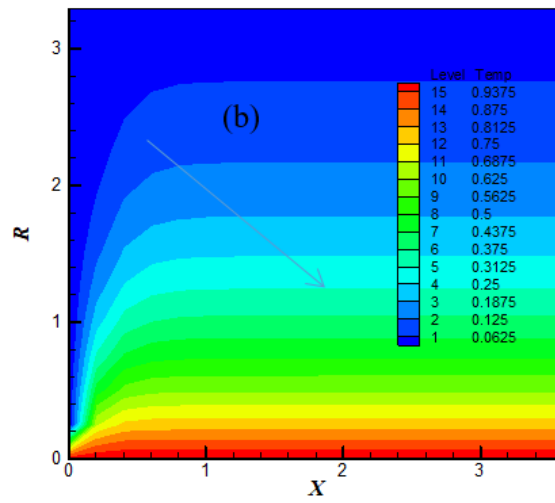


Figure 18. (b) Isotherms flood view

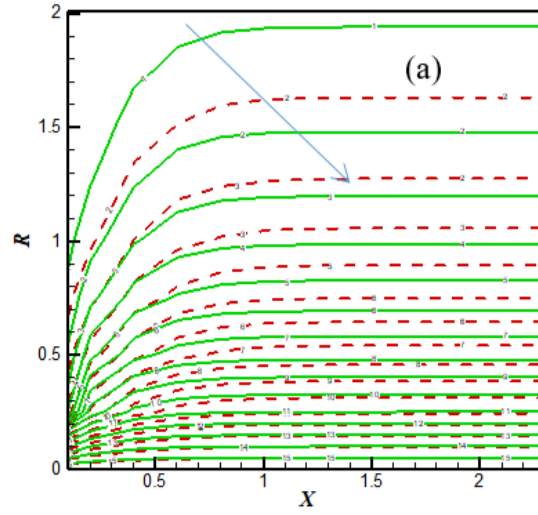


Figure 19. (a) Isotherms for $Pr = 2.1$ (red dashed line) and $Pr = 1.2$ (green solid line)

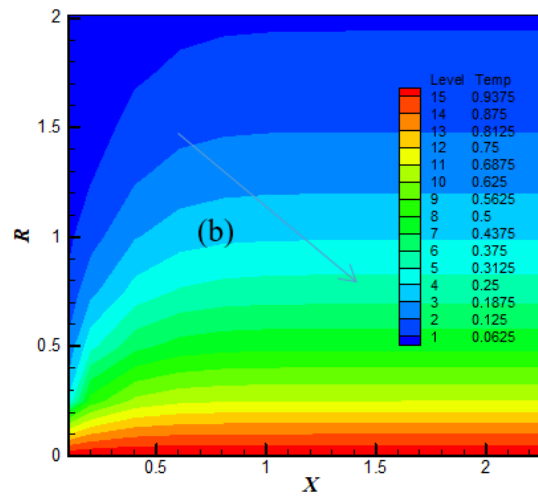


Figure 19. (b) Isotherms flood view

Table 2. Computational numerical values with the changes of β and M for skin friction and Nusselt number

β	Cf	Nu	M	Cf	Nu
0.7	-0.79393	2.04655	0.0	-0.84090	2.04655
1.4	-0.94995	2.04655	1.0	-1.01627	2.04655
2.0	-1.01627	2.04655	2.0	-1.15432	2.04655
3.0	-1.07788	2.04655	3.0	-1.27028	2.04655

Table 3. provides the numerical values of skin friction and Nusselt number effects of Brownian parameter, Nb, thermophoresis parameter, Nt and Prandtl number, Pr. It is clear that only Nusselt number changes for rising values of Nb, Nt and Pr.

Table 3. Computational numerical values of skin friction and Nusselt number for Nb, Nt and Pr.

Nb	Nt	Pr	Cf	Nu
0.1			-1.01627	2.04655
0.3			-1.01627	2.01020
0.5			-1.01627	1.97417
0.7			-1.01627	1.93849
	0.2		-1.01627	2.01214
	0.4		-1.01627	1.98006
	0.6		-1.01627	1.94842
	0.8		-1.01627	1.91722
		0.7	-1.01627	2.04655
		3.0	-1.01627	2.00658
		7.0	-1.01627	2.02565

6. Conclusions

From the current numerical inquisition, the subsequent conclusions have been skimmed:

- With the increase of Casson fluid parameter and magnetic parameter, the momentum boundary layers decrease.
- Thermal boundary layers increase for the increase of both Brownian parameter and thermophoresis parameter.
- For the increment of thermophoresis parameter, concentration profiles increase but decrease with the raise of Lewis number.

- Skin friction profiles decrease with the improvement of both Casson fluid parameter and magnetic parameter.
- The effect of Brownian parameter, thermophoresis parameter and Prandtl number, Nusselt number decrease.
- With the increase of Casson fluid parameter, streamlines decrease but increase with the increase of magnetic parameter.
- Isotherms increase with the increase of both Brownian parameter and thermophoresis parameter but decrease according to Prandtl number increases.

References

- Boyd J., Buick J. M., Green S. (2007). Analysis of Casson and Carreau – Yasuda non-Newtonian blood models in steady and oscillatory flow using the lattice Boltzmann method. *Phys. Fluids*, Vol. 19, pp. 93-103. <https://doi.org/10.1063/1.2772250>
- Buongiorno J. (2006). Convective transport in nano-fluids. *Journal of Heat Transfer*, Vol. 128, pp. 240-250. <https://doi.org/10.1115/1.2150834>
- Casson N. (1959). A flow equation for pigment oil suspensions of the printing ink type. In: Rheology of Disperse Systems, Mill, C. C. (Ed.), *Advances in Mechanical Engineering*, Pergamon Press, Oxford, pp. 84-104.
- Chevalley J. (1991). An adaptation of Casson equation for the rheology of chocolate. *J. Texture Studies*, Vol. 22, pp. 219-229. <https://doi.org/10.1111/j.1745-4603.1991.tb00015.x>
- Choi S. (1995). Enhancing thermal conductivity of fluids with nano-particles. *ASME-Publi. Fed.*, Vol. 231, pp. 99-105. <https://www.osti.gov/servlets/purl/196525>
- Cokelet G., Shin H., Britten A., Wells R. E. (1963). Rheology of human blood – measurement near and at zero shear rate. *Trans. Soc. Rheol.*, Vol. 7, pp. 303-317. <https://doi.org/10.1122/1.548959>
- Eldabe N. T. M., Salwa M. G. E. (1995). Heat transfer of MHD non-Newtonian Casson fluid flow between two rotating cylinder. *J. Phys. Soc. Jpn.*, Vol. 64, pp. 41-64.
- Emmanuel M. A., Ibrahim Y. S., Letis B. B. (2015). Analysis of Casson fluid flow over a vertical porous surface with chemical reaction in the presence of magnetic field. *Journal of Applied Mathematics*, Vol. 3, pp. 713-723. <https://doi.org/10.4236/jamp.2015.36085>
- Garcia-Ochoa F., Casa J. A. (1994). Apparent yield stress in xanthium gum solutions at low concentrations. *Chem. Eng. J.*, Vol. 53, pp. B41-B46. [https://doi.org/10.1016/0923-0467\(93\)06043-P](https://doi.org/10.1016/0923-0467(93)06043-P)
- Hayat T., Bilal A. M., Shehzad S. A., Alsaedi A. (2015). Mixed convection flow of Casson nanofluid over a stretching sheet with convectively heated chemical reaction and heat source/sink. *Journal of Applied Fluid Mechanics*, Vol. 8, pp. 803-811. <https://doi.org/10.18869/acadpub.jafm.67.223.22995>
- Hussanan A., Zukhi S. M., Tahar R. M., Khan I. (2014). Unsteady boundary layer flow and heat and mass transfer of a Casson fluid past an oscillating vertical plate with Newtonian heating. *PLOS ONE*, Vol. 9, pp. e108763. <https://doi.org/10.1371/journal.pone.0108763>

- Kataria H. R., Patal H. R. (2016). Soret and heat generation effects on MHD Casson fluid flow past an oscillating vertical plate embedded through porous medium. *Alexandria Engineering Journal*, Vol. 55, pp. 2125-2137. <https://doi.org/10.1016/j.aej.2016.06.024>
- Kataria H. R., Patel H. R. (2016). Radiation and chemical reaction effects on MHD Casson fluid flow past an oscillating vertical plate embedded in porous medium. *Alexandria Engineering Journal*, Vol. 55, pp. 583-595. <https://doi.org/10.1016/j.aej.2016.01.019>
- Khan M. S., Karim I., Ali L. E., Islam A. (2012). Unsteady MHD free convection boundary-layer flow of a nanofluid along a stretching sheet with thermal radiation and viscous dissipation effects. *International Nano Letters*, Vol. 2, pp. 24. <https://doi.org/10.1186/2228-5326-2-24>
- Kumari P. K., Murthy M. V., Reddy M., Kumar Y. V. K. (2011). Peristaltic pumping of a magnetohydrodynamic Casson fluid in an inclined channel. *Adv. Appl. Sci. Res.*, Vol. 2, pp. 428-436.
- Mahabaleshwar U., Lorenzini G. (2017). Combined effect of heat source/sink and stress work on MHD Newtonian fluid flow over a stretching porous sheet. *International Journal of Heat and Technology*, Vol. 35, pp. 330-S335. <https://doi.org/10.18280/ijht.35Sp0145>
- Makanda G., Shaw S., Sibanda P. (2015). Effects of radiation on MHD free convection of a Casson fluid from a horizontal circular cylinder with partial slip in non-Darcy porous medium with viscous dissipation. *Boundary Value Problems*, pp. 75. <https://doi.org/10.1186/s13661-015-0333-5>
- Malik M. Y., Naseer M., Nadeem S., Rehman A. (2014). The boundary layer flow of Casson nanofluid over a vertical exponentially stretching cylinder. *Applied Nanoscience*, Vol. 4, pp. 869-873. <https://doi.org/10.1007/s13204-013-0267-0>
- Nadeem S., Haq R. U., Lee C. (2012). MHD flow of Casson fluid over an exponentially shrinking sheet. *Scientia Iranica*, Vol. 19, pp. 1550-1553. <https://doi.org/10.1016/j.scient.2012.10.021>
- Okay S. (1979). Non-Newtonian blood flow in capillary with a permeable wall. In: Proc. Festschrift of Harold Wayland Symposium, *California Inst. Of Tech.*, Pasadena, USA.
- Sakiadis B. C. (1961). Boundary layer behavior on continuous solid surface: 1. Boundary-layer equations for two-dimensional and axisymmetric flow. *AIChE Journal*, Vol. 7, No. 1, pp. 26-28. <https://doi.org/10.1002/aic.690070108>
- Sreenadh S., Pallavi A. R., Satynarayana B. (2011). Flow of a Casson fluid through an inclined tube of non-uniform cross section with multiple stenosis. *Adv. Appl. Sci. Res.*, Vol. 2, No. 5, pp. 340-349.
- Walwander W. P., Chen T. Y., Cala D. F. (1975). An approximate Casson fluid model for tube flow of blood. *Biorheology*, Vol. 12, pp. 111-119. <https://doi.org/10.3233/BIR-1975-12202>

Nomenclature

B_0	External magnetic field, [Wbm^{-2}]
C	Dimensionless concentration, [-]
C_f	Skin friction, [-]
\bar{C}	Concentration component

C_p	Specific heat at constant pressure, [$\text{Jkg}^{-1}\text{K}^{-1}$]
\bar{C}_w	Concentration of the cylinder, [mol.]
\bar{C}_∞	Concentration away from the cylinder
D_B	Brownian diffusion coefficient
D_T	thermophoresis diffusion coefficient
Le	Lewis number, [-]
M	Magnetic parameter, [-]
Nb	Brownian parameter, [-]
Nt	Thermophoresis parameter, [-]
Nu	Nusselt number, [-]
Pr	Prandtl number, [-]
Sh	Sherwood number, [-]
T	Non-dimensional temperature, [-]
\bar{T}	Temperature, [K]
\bar{T}_∞	Temperature away from the cylinder
\bar{T}_w	Temperature of the fluid
\bar{t}	Dimensional time, [s]
t	Non-dimensional time, [-]
u_0	Uniform velocity, [ms^{-1}]
U	Non-dimensional velocity, [-]
u, v	Dimensional velocity of the fluid in x and r direction
x, r	Coordinate axis alone and normal to the cylinder
X, R	Non-dimensional coordinate axis alone and normal to the cylinder

Greek symbols

β	Casson parameter, [-]
Γ	Rate time constant, [s]
κ	Thermal conductivity, [$\text{Wm}^{-1}\text{K}^{-1}$]
ρ	Density, [kgm^{-3}]
ν	Kinematic viscosity, [m^2s^{-1}]

